

Using the singular value decomposition to extract 2D correlation functions from scattering patterns

PHILIPP BENDER,^{a*} DOMINIKA ZÁKUTNA,^{b,c} SABRINA DISCH,^c
LOURDES MARCANO,^{d,e} DIEGO ALBA VENERO^f AND DIRK HONECKER^b

^a*Physics and Materials Science Research Unit, University of Luxembourg,
162A avenue de la Faïencerie, L-1511 Luxembourg, Grand Duchy of Luxembourg,*

^b*Large Scale Structures group, Institut Laue-Langevin, 71 avenue des Martyrs,*

*F-38042 Grenoble, France, ^cDepartment für Chemie, Universität zu Köln,
Luxemburger Strasse 116, D-50939 Köln, Germany, ^dHelmholtz-Zentrum Berlin für*

Materialien und Energie, Albert-Einstein-Strasse 15, D-12489 Berlin Germany,

^e*Departamento Electricidad y Electrnica, Universidad del Pas Vasco UPV/EHU,
E-48940 Leioa, Spain, and ^fISIS Neutron and Muon Facility, Rutherford Appleton
Laboratory, Chilton, OX11 0QX, United Kingdom. E-mail: philipp.bender@uni.lu*

small-angle scattering; correlation function; two-dimensional Fourier transform; anisotropic structures;

nanoparticles; singular value decomposition; noise filtering

Abstract

We apply the truncated singular value decomposition (SVD) to extract the underlying 2D correlation functions from small-angle scattering patterns. We test the approach by transforming the simulated data of ellipsoidal particles and show that also in case of anisotropic patterns (i.e. aligned ellipsoids) the derived correlation functions correspond to the theoretically predicted profiles. Furthermore, we use the truncated SVD

to analyze the small-angle x-ray scattering patterns of colloidal dispersions of hematite spindles and magnetotactic bacteria in presence of magnetic fields, to verify that this approach can be applied to extract model-free the scattering profiles of anisotropic scatterers from noisy data.

1. Introduction

Small-angle angle scattering of x-rays (SAXS) or neutrons (SANS) is routinely used to investigate the structural properties of various materials, such as nanostructured bulk samples (Fritz-Popovski, 2013; Fritz-Popovski, 2015; Michels, 2014) or nanoparticle ensembles (Reufer *et al.*, 2010; Märkert *et al.*, 2011; Hoffelner *et al.*, 2015; Nack *et al.*, 2018). In many cases, the detected 2D scattering patterns $I(\mathbf{q})$ (here I is the scattering intensity and \mathbf{q} the scattering vector on the 2D detector plane), are isotropic and data analysis is performed on the 1D azimuthal average $I(q)$, by either fitting it in reciprocal space with model functions or by transforming $I(q)$ to real-space correlation functions $C(r)$ *via* Fourier transforms (FT) (Pedersen, 1997). For the latter, a direct FT can be used (Michels *et al.*, 2003) or, alternatively, an indirect FT (Glatter, 1977; Hansen, 2000; Bender *et al.*, 2017). Often the pair distance distribution function $P(r) = C(r)r^2$ is determined, which gives direct information about the average shape, size and structure of the scattering units (Glatter, 1979; Svergun & Koch, 2003). In case of anisotropic nanostructures, the pattern $I(\mathbf{q})$ can be anisotropic, provided the nanostructures are preferentially aligned along a certain director or texture axis (Van der Heijden *et al.*, 2004; Reufer *et al.*, 2010; Märkert *et al.*, 2011; Fritz-Popovski, 2013; Hoffelner *et al.*, 2015; Nack *et al.*, 2018). Also in this case data analysis can be either performed by adjusting the whole scattering pattern in reciprocal space (Alves *et al.*, 2017) or by transforming the pattern *via* 2D FTs to the real-space 2D correlation functions (Fritz-Popovski, 2013; Fritz-

Popovski, 2015; Mettus & Michels, 2015). For the indirect 2D FT proposed in Fritz-Popovski (2013), regularization functionals are appended to the system matrix, which is necessary to obtain smooth profiles, but which can increase the computation times significantly. Here, we propose a similar but faster method, namely the truncated singular value decomposition (SVD), to extract the underlying 2D correlation functions. We propose that this method could be used for live, model-free data analysis, e.g. in capillary flow devices (Nielsen *et al.*, 2012), time-resolved nanoparticle-oscillation (Bender *et al.*, 2015) or rheo-SAXS/SANS experiments (Panine *et al.*, 2003; Calabrese *et al.*, 2016), and microfluidics (Stehle *et al.*, 2013; Poulos *et al.*, 2016; Adamo *et al.*, 2018), where the noise reduction of the SVD helps to enhance the signal.

2. Methods

2.1. Singular value decomposition SVD

In polar coordinates the 2D scattering intensity $I(q_y, q_z) = I(q, \Theta)$ (the beam is along the x -direction, $\mathbf{k} \parallel \mathbf{e}_x$) is a function of the magnitude of the scattering vector $|\mathbf{q}|$ and the angle Θ . With $i = N$ unique data points (i.e. pixels of the detector for a monochromatic source) it can be written

$$I(q_i, \Theta_i) = \sum_{k=1}^K A_{ik} P(r_k, \varphi_k), \quad (1)$$

where the angle φ specifies the orientation of \mathbf{r} in real space in the yz plane. Here, the extracted 2D distribution function is $P(r, \varphi) = C(r, \varphi)r$ (Fritz-Popovski, 2013), and the matrix \mathbf{A} has the elements (Mettus & Michels, 2015)

$$A_{ik} = \cos(q_i r_k \cos(\Theta_i - \varphi_k)) \Delta r_k \Delta \varphi_k. \quad (2)$$

Here, we usually assume a linear spacing for the pre-determined r - and φ -vectors (i.e. Δr and $\Delta \varphi = \text{const}$). By minimizing the deviation (i.e. performing a least-square fit)

$$\chi^2 = \sum_{i=1}^N \frac{(I(q_i, \Theta_i) - \sum_{k=1}^K A_{ik} P(r_k, \varphi_k))^2}{\sigma_i^2} \quad (3)$$

the 2D correlation function $P(r, \varphi) = C(r, \varphi)r$ can be determined. In case of significant measurement uncertainties σ_i , however, this distribution will exhibit strong, unphysical oscillations. While performing the indirect Fourier transform, regularization matrices are appended (e.g. a Tikhonov regularization can be applied) to force smooth distributions (Fritz-Popovski, 2013), and various approaches exist to estimate the optimal value for the regularization parameter (Glatter, 1977; Hansen, 2000).

With the SVD the decomposition of the system matrix $\mathbf{A} = \mathbf{U}\mathbf{S}\mathbf{V}^T$ is performed, where \mathbf{U} and \mathbf{V} are orthogonal $N \times N$ and $K \times K$ matrices, respectively, and \mathbf{S} is a $N \times K$ matrix whose main diagonal elements $s_i \equiv s_{ii}$ are the singular values (all other values are zeros). The solution $P(r, \varphi)$ of the functional $\mathbf{A}P(r, \varphi) = I(q, \Theta)$ is

$$P(r, \varphi) = \mathbf{V}\mathbf{S}^+\mathbf{U}^T I(q, \Theta), \quad (4)$$

where \mathbf{S}^+ has the reciprocal values $1/s_i$ in its diagonal, and otherwise zeros. Using the full-rank matrices for the reconstruction of $P(r, \varphi)$ according to Eq. 4 should result in the same distribution as minimizing Eq. 3. In particular, very small s_i values associated to noise result in strong oscillations of the reconstructed distribution. Thus, a smoothing of $P(r, \varphi)$ can be achieved by reducing the number of singular values s_i that are considered for \mathbf{S}^+ (Berkov *et al.*, 2000) (i.e. singular values which are smaller than a certain threshold are set to zero). Alternatively, a truncated SVD can be performed (Hansen, 1987; Viereck *et al.*, 2019), which further reduces the computation time compared to a SVD of the full-ranked matrices.

We will use the truncated SVD to analyze first the simulated scattering patterns of an ensemble of prolate ellipsoids and later the measured SAXS patterns of a colloidal dispersion of hematite spindles and of magnetotactic bacteria.

2.2. Samples

Details regarding the synthesis and characterization of the hematite spindles can be found in (Zákutná *et al.*, 2019). Hematite nanospindles are weakly ferromagnetic and known to orient with their main axis perpendicular to an applied magnetic field (Reufer *et al.*, 2010; Märkert *et al.*, 2011; Roeder *et al.*, 2015; Hoffelner *et al.*, 2015; Nack *et al.*, 2018). According to electron microscopy, the sample studied here has a length of the short spindle axes of around 56 nm and of the long axis of around 375 nm. The SAXS measurements from (Zákutná *et al.*, 2019), which we also analyze here, were performed at the ID02 instrument at the ESRF (Narayanan *et al.*, 2018) on a dilute, i.e. non-interacting, dispersion of the nanospindles. A static homogeneous magnetic field up to 520 mT was applied with an electromagnet in horizontal direction perpendicular to the incoming beam.

A detailed study of the magnetotactic bacteria is presented in (Orue *et al.*, 2018). These bacteria contain on average about 15-20 iron oxide nanoparticles with diameters of around 40-50 nm, which are typically arranged in nearly linear chains. Here we analyze a SAXS measurement of the same colloidal dispersion of bacteria as presented in Orue *et al.* (2018). This measurement was performed with a Xenocs Nano-InXider. The colloidal dispersion was filled into a quartz glass capillary and the bacteria aligned perpendicular to the incoming beam by positioning a small permanent magnet next to the capillary. With this setup only one full quadrant of the pattern is detected but assuming symmetry the total 2π pattern can be easily reconstructed.

3. Results

3.1. Simulated data

To test the truncated SVD, we first analyze the calculated scattering patterns of rotational ellipsoids with an equatorial radius of 50 nm and a polar radius of 150 nm

(*Left column* in Figs. 1(a) and (b)). In Fig. 1(a) (upper row) we analyze the isotropic ensemble and in Fig. 1(b) (lower row) the anisotropic ensemble. The simulated scattering patterns had $N = 30480$ data points, and we calculated the system matrix \mathbf{A} (30480×10224 matrix) for 101 r -values ($0 - 400$ nm, 1 nm-steps) and 144 φ -values ($2.5 - 360^\circ$, 2.5° -steps). We then varied the number of singular values N_s considered for the reconstruction. As shown in Fig. 2(a), the total error χ^2 is significantly reduced by increasing N_s and exhibits a minimum at around $N_s = 1180$, which is marked by the dashed line (here we used $\sigma_i^2 = I(q_i, \Theta_i)$ for the calculation of χ^2 , Eq. 3). Further increasing N_s does not minimize the deviations more, but will generate strong oscillations due to the restricted q -range (Qiu *et al.*, 2004). In Fig. 1 we plot the reconstructed distributions for $N_s = 1180$, and in case of the anisotropic ensemble compare them to the theoretically expected profiles $C(r)r$ (Fritz-Popovski, 2015), which we calculated for spheres with diameters of 100 nm and 300 nm, respectively. The good agreement shows that the truncated SVD can be readily used to extract fast the underlying 2D correlation functions from 2D scattering patterns, at least in case of smooth data.

3.2. Experimental data

3.2.1. *Hematite spindles* In Fig. 3 we show the analysis results of the field-dependent scattering patterns of the colloidal dispersion of hematite spindles. In the upper row (Fig. 3(a)) we display the results for 0 mT and in the lower row (Fig. 3(b)) the results for $\mu_0 H = 520$ mT. For both, the isotropic and the anisotropic pattern, the SVD was performed for 101 r -values ($0 - 400$ nm) and 144 φ -values ($2.5 - 360^\circ$, 2.5° -steps). The correlation functions plotted in Fig. 3 were determined for $N_s = 1270$, for which the total error was already close to the minimum (Fig. 2(b)). For both cases the extracted correlation functions exhibit some oscillations, but which increases significantly with increasing N_s (i.e. smaller singular values are associated to signal noise).

At 0 mT, the anisotropic particles are randomly oriented within the viscous matrix (water), and thus the scattering pattern and the derived correlation function are both isotropic. The extracted profile has a pronounced peak at around 50 nm and a long tail, and hence corresponds well to the expected profile of randomly-oriented, shape-anisotropic nanoparticles (Svergun & Koch, 2003).

At 520 mT on the other hand, the particle moments are mostly oriented in field direction. The dominance of the magnetocrystalline anisotropy leads to a net magnetic moment in the basal plane of the hematite spindles, i.e. perpendicular to the long particle axis (Reufer *et al.*, 2010; Hoffelner *et al.*, 2015; Nack *et al.*, 2018). Therefore, the long spindle axes are oriented within the plane perpendicular to the field direction, which explains the anisotropy of both the scattering pattern and the extracted correlation function. Along $\varphi = 90^\circ$ (*right column* of Fig. 3(b)) the profile indicates a maximum length of the spindles of around 400 nm, whereas the profile along $\varphi = 0^\circ$ agrees well with the expected correlation function for spindles with an equatorial radius of 56 nm. Thus, the extracted 2D correlation function is in good agreement with our previous results (Zákutná *et al.*, 2019).

3.2.2. Magnetotactic bacteria In Fig. 4 we show the highly anisotropic SAXS pattern of the aligned magnetotactic bacteria along the horizontal field direction. The extracted correlation function was determined, as before, for 101 r -values (0 – 200 nm) and 144 φ -values (2.5° – 360° , 2.5° -steps). The function plotted in Fig. 4 was determined for $N_s = 1000$, which shows that the particles are preferentially spheres (radially symmetric spots), and that the bacteria and thus the magnetosome chains are well aligned along the applied field showing no spreading of the spots in the azimuthal direction. From the profile along $\varphi = 0^\circ$ (*right column* of Fig. 4) we can estimate the average center-to-center distance between the particles in the chain from the peak-

to-peak distance to be around 50 nm and the particle size from the peak width to be around 40 nm, which agrees well with previous results (Orue *et al.*, 2018). Along $\varphi = 90^\circ$ we only see the cross section of a single particle, and the profile takes on negative values which we attribute to a lower scattering length density in the vicinity of the particle (inside the bacteria) compared to the surrounding matrix.

4. Conclusions

Here, we introduce the truncated singular value decomposition (SVD) to extract the denoised two-dimensional correlation functions from small-angle scattering patterns. First, we analyze simulated data of ellipsoidal particles and show that the derived correlation functions correspond well to the theoretically predicted profiles. Furthermore, we use this method to successfully extract the underlying 2D correlation functions from experimental SAXS patterns of colloidal dispersions of hematite spindles and magnetotactic bacteria. We emphasize that this method is a fast and easy way to obtain model-free information about the structural properties of anisotropic scatterers, which we propose for example for the analysis of live data.

P. Bender acknowledges financial support from the National Research Fund of Luxembourg (CORE SANS4NCC grants), L. Marcano acknowledges the Basque Government for her fellowship (POS_2018_1_0070) and S. Disch acknowledges financial support from the German Research Foundation (DFG: DI 1788/2-1). The SAXS experiments on the hematite spindles were performed on beamline ID02 at the European Synchrotron Radiation Facility (ESRF), Grenoble, France, and we are grateful to Sylvain Prvost for providing assistance. We thank the group of Magnetism and Magnetic Materials at the Universidad del Pas Vasco for preparing the magnetotactic bacteria and the Science and Technology Facilities Council (STFC) for access to the SAXS kit at the Materials Characterisation Laboratory to perform the SAXS measurement.

References

Adamo, M., Poulos, A. S., Lopez, C. G., Martel, A., Porcar, L. & Cabral, J. T. (2018). *Soft Matter*, **14**(10), 1759–1770.

Alves, C., Pedersen, J. S. & Oliveira, C. L. (2017). *J. Appl. Crystallogr.* **50**(3), 840–850.

Bender, P., Bogart, L. K., Posth, O., Szczerba, W., Rogers, S. E., Castro, A., Nilsson, L., Zeng, L. J., Sugunan, A., Sommertunge, J., Fornara, A., González-Alonso, D., Fernández Barquín, L. & Johansson, C. (2017). *Sci. Rep.* **7**, 45990.

Bender, P., Günther, A., Honecker, D., Wiedenmann, A., Disch, S., Tschöpe, A., Michels, A. & Birringer, R. (2015). *Nanoscale*, **7**(40), 17122–17130.

Berkov, D. V., Görnert, P., Buske, N., Gansau, C., Mueller, J., Giersig, M., Neumann, W. & Su, D. (2000). *J. Phys. D: Appl. Phys.* **33**(4), 331.

Calabrese, M. A., Wagner, N. J. & Rogers, S. A. (2016). *Soft Matter*, **12**(8), 2301–2308.

Fritz-Popovski, G. (2013). *J. Appl. Crystallogr.* **46**(5), 1447–1454.

Fritz-Popovski, G. (2015). *J. Appl. Crystallogr.* **48**(1), 44–51.

Glatter, O. (1977). *J. Appl. Crystallogr.* **10**(5), 415–421.

Glatter, O. (1979). *J. Appl. Crystallogr.* **12**(2), 166–175.

Hansen, P. C. (1987). *BIT*, **27**(4), 534–553.

Hansen, S. (2000). *J. Appl. Crystallogr.* **33**(6), 1415–1421.

Van der Heijden, P., Rubatat, L. & Diat, O. (2004). *Macromolecules*, **37**(14), 5327–5336.

Hoffelner, D., Kundt, M., Schmidt, A. M., Kentzinger, E., Bender, P. & Disch, S. (2015). *Faraday Discuss.* **181**, 449–461.

Märkert, C., Fischer, B. & Wagner, J. (2011). *J. Appl. Crystallogr.* **44**(3), 441–447.

Mettus, D. & Michels, A. (2015). *J. Appl. Crystallogr.* **48**(5), 1437–1450.

Michels, A. (2014). *J. Phys.: Condens. Matter*, **26**(38), 383201.

Michels, A., Viswanath, R. N., Barker, J. G., Birringer, R. & Weissmüller, J. (2003). *Phys. Rev. Lett.* **91**(26), 267204.

Nack, A., Seifert, J., Passow, C. & Wagner, J. (2018). *J. Appl. Crystallogr.* **51**(1), 87–96.

Narayanan, T., Sztucki, M., Van Vaerenbergh, P., Léonardon, J., Gorini, J., Claustre, L., Sever, F., Morse, J. & Boesecke, P. (2018). *J. Appl. Crystallogr.* **51**(6).

Nielsen, S. S., Møller, M. & Gillilan, R. E. (2012). *J. Appl. Crystallogr.* **45**(2), 213–223.

Orue, I., Marcano, L., Bender, P., García-Prieto, A., Valencia, S., Mawass, M., Gil-Cartón, D., Venero, D. A., Honecker, D., García-Arribas, A., Fernández Barquín, L., Muela, A. & Fdez-Gubieda, M. (2018). *Nanoscale*, **10**(16), 7407–7419.

Panine, P., Gradzielski, M. & Narayanan, T. (2003). *Rev. Sci. Instrum.* **74**(4), 2451–2455.

Pedersen, J. S. (1997). *Adv. Colloid Interface Sci.* **70**, 171–210.

Poulos, A. S., Nania, M., Lapham, P., Miller, R. M., Smith, A. J., Tantawy, H., Caragay, J., Gummel, J., Ces, O., Robles, E. S. & Cabral, J. T. (2016). *Langmuir*, **32**(23), 5852–5861.

Qiu, X., Thompson, J. W. & Billinge, S. J. (2004). *J. Appl. Crystallogr.* **37**(4), 678–678.

Reufer, M., Dietsch, H., Gasser, U., Hirt, A., Menzel, A. & Schurtenberger, P. (2010). *J. Phys. Chem. B*, **114**(14), 4763–4769.

Roeder, L., Bender, P., Kundt, M., Tschöpe, A. & Schmidt, A. M. (2015). *Phys. Chem. Chem. Phys.* **17**(2), 1290–1298.

Stehle, R., Goerigk, G., Wallacher, D., Ballauff, M. & Seiffert, S. (2013). *Lab Chip*, **13**(8), 1529–1537.

Svergun, D. I. & Koch, M. H. J. (2003). *Rep. Prog. Phys.* **66**(10), 1735.

Viereck, T., Draack, S., Schilling, M. & Ludwig, F. (2019). *J. Magn. Magn. Mater.* **475**, 647–651.

Zákonutná, D., Falke, Y., Dresen, D., Prévost, S., Bender, P., Honecker, D. & Disch, S. (2019). *Nanoscale*, **11**, Advance Article.

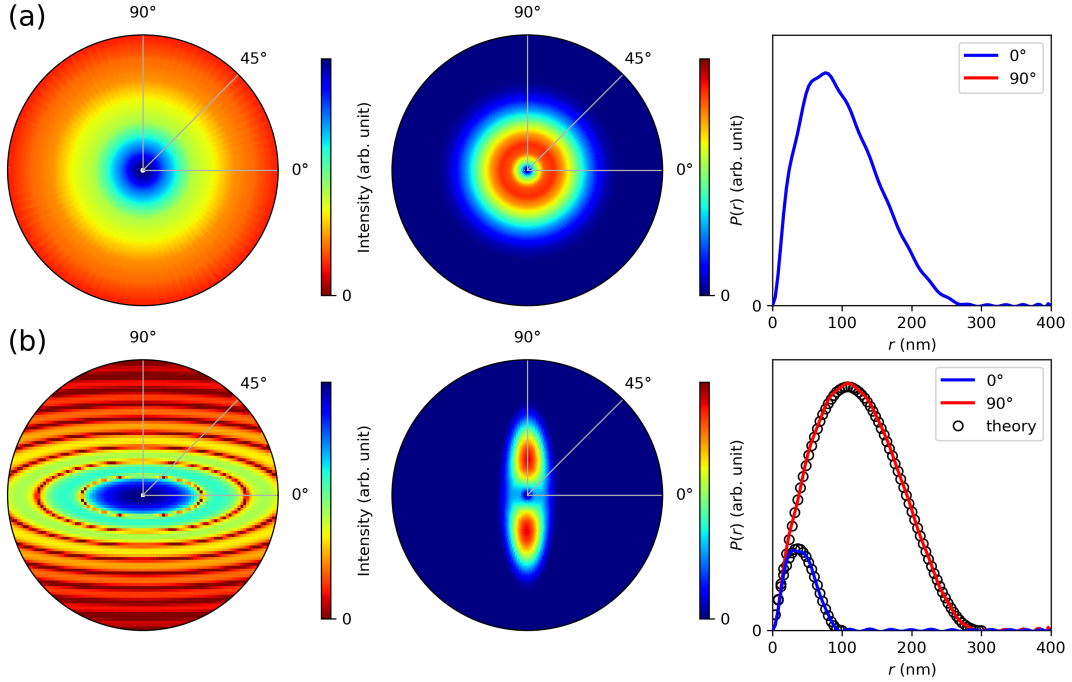


Fig. 1. Determination of the 2D correlation functions by a SVD for a monodisperse ensemble of prolate rotational ellipsoids with an equatorial radius of 50 nm and a polar radius of 150 nm. (a) Ellipsoids are randomly oriented (isotropic ensemble). (b) Ellipsoids are aligned with their polar axis along $\Theta = 90^\circ$ (anisotropic ensemble). *Left column:* Polar plot of the scattering pattern in logarithmic scale ($q_{\max} = 0.2 \text{ nm}^{-1}$). *Middle column:* Extracted 2D correlation function $P(r, \varphi)$ ($r_{\max} = 400 \text{ nm}$). *Right column:* Correlation function along $\varphi = 0^\circ$ and 90° , and in (b) additionally the calculated cross sections for spheres with diameters of 100 nm and 300 nm, respectively.

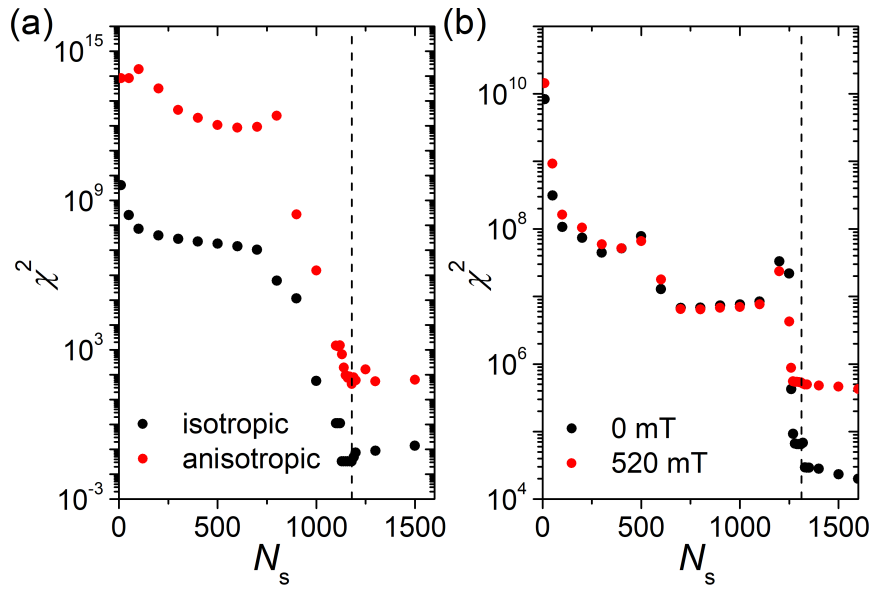


Fig. 2. Error χ^2 (Eq. 3) for the fit of (a) the simulated data (Fig. 1), and (b) the experimental data of the spindles (Fig. 3) at two different fields, with N_s being the number of singular values used for the reconstruction.

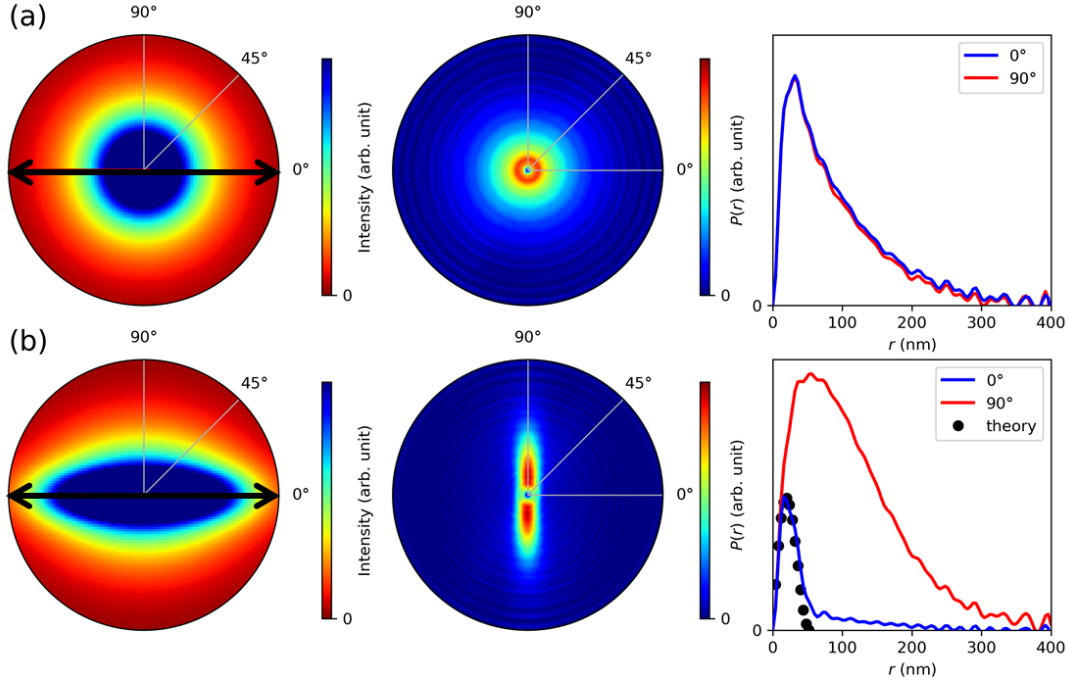


Fig. 3. Analysis of the 2D SAXS patterns of the colloidal dispersion of hematite spinules; the magnetic field was applied in horizontal direction ($\Theta = 0^\circ$) with a field strength of (a) 0 mT and (b) 520 mT. *Left column*: Polar plot of the scattering pattern in logarithmic scale ($q_{\max} = 0.1 \text{ nm}^{-1}$). *Middle column*: Extracted 2D correlation function $P(r, \varphi)$ ($r_{\max} = 400 \text{ nm}$). *Right column*: Correlation function along $\varphi = 0^\circ$ and 90° , and the theoretically expected cross sections for a sphere with a diameter of 56 nm (black dots).

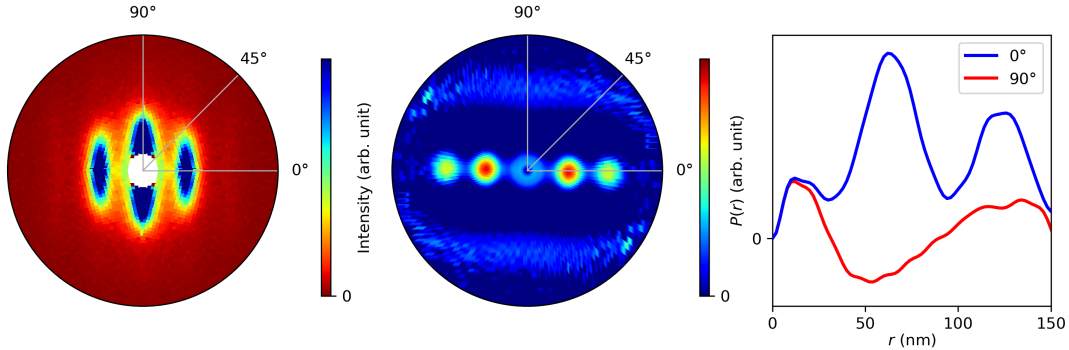


Fig. 4. Analysis of the 2D SAXS pattern of the colloidal dispersion of magnetotactic bacteria; the magnetic field was applied in horizontal direction ($\Theta = 0^\circ$). *Left column*: Polar plot of the scattering pattern in logarithmic scale ($q_{\max} = 0.5 \text{ nm}^{-1}$). *Middle column*: Extracted 2D correlation function $P(r, \varphi)$ ($r_{\max} = 150 \text{ nm}$). *Right column*: Correlation function along $\varphi = 0^\circ$ and 90° .

Synopsis

We apply the truncated singular value decomposition (SVD) to extract the underlying 2D correlation functions from small-angle scattering patterns.
